Generating, Separating and Polarizing Terahertz Vortex Beams via Liquid Crystals with Gradient-Rotation Directors

Shi-Jun Ge [1], Zhi-Xiong Shen [1], Peng Chen [1], Xiao Liang [2],*, Xin-Ke Wang [3], Wei Hu [1],* iD **, Yan Zhang [3] and Yan-Qing Lu [1]**

[1] National Laboratory of Solid State Microstructures, Collaborative Innovation Center of Advanced Microstructures and College of Engineering and Applied Sciences, Nanjing University, Nanjing 210093, China; gsj091190023@163.com (S.-J.G.); njuzxshen@163.com (Z.-X.S.); ndclchuangxinjihua@163.com (P.C.); yqlu@nju.edu.cn (Y.-Q.L.)
[2] Department of Chemistry, Tsinghua University, Beijing 100084, China
[3] Department of Physics, Capital Normal University, Beijing Key Laboratory of Metamaterials and Devices, Key Laboratory of Terahertz Optoelectronics, Ministry of Education, and Beijing Advanced Innovation Center for Imaging Technology, Beijing 100048, China; wxk82721@cnu.edu.cn (X.-K.W.); yzhang@cnu.edu.cn (Y.Z.)
* Correspondence: liangxiao@tsinghua.edu.cn (X.L.); huwei@nju.edu.cn (W.H.); Tel.: +86-25-8359-7400 (W.H.)

Abstract: Liquid crystal (LC) is a promising candidate for terahertz (THz) devices. Recently, LC has been introduced to generate THz vortex beams. However, the efficiency is intensely dependent on the incident wavelength, and the transformed THz vortex beam is usually mixed with the residual component. Thus, a separating process is indispensable. Here, we introduce a gradient blazed phase, and propose a THz LC forked polarization grating that can simultaneously generate and separate pure THz vortices with opposite circular polarization. The specific LC gradient-rotation directors are implemented by a photoalignment technique. The generated THz vortex beams are characterized with a THz imaging system, verifying features of polarization controllability. This work may pave a practical road towards generating, separating and polarizing THz vortex beams, and may prompt applications in THz communications, sensing and imaging.

1. Introduction

Vortex beams, which feature a spiral wavefront, have gained considerable interest in recent years [1,2]. In contrast to the spin angular momentum (SAM) related to circular polarization, a vortex beam carries orbital angular momentum (OAM) [3]. OAM is quantized as $m\hbar$ per photon, where m is the topological charge, indicating how many twists the light performs in one wavelength. OAM adds another degree of freedom in the manipulation of light. The OAM-induced torque and abundant eigenstates lead to numerous applications, such as optical tweezers [4], optical communications [5,6], quantum entanglement [7], and informatics [8,9]. Beyond the optical band, the concept of the vortex beam has also been extended to much broader spectra; the terahertz (THz) range.

THz waves, typically defined as electromagnetic waves in the frequency range of 0.1~10 THz, are very promising for versatile applications in security screening, material characterization, and nondestructive inspection [10,11]. In particular, THz vortex beams are attractive for applications in

sensing, wireless communication, and manipulation of a quantum condensate [12,13]. Several methods, including spiral phase plates [14,15], computer-generated holograms [16,17], metasurfaces [18], and Pancharatnam-Berry phase optical elements (PBOEs) [19,20] have been implemented to generate THz vortex beams; however, they are either fixed without tunability and switchability, or suffer from low efficiency. Liquid crystal (LC) is an excellent candidate for THz devices [21–28]. Recently, we demonstrated a THz q-plate by introducing a large-birefringence LC to generate THz vortex beams [29]. However, the efficiency was intensely dependent on the incident wavelength, and the generated vortex beams were usually impure, in mixed states with unconverted beam components. Thus, an additional separating process is indispensable, making the setup more complicated and untalented.

In this work, we introduce a gradient blazed phase into the vortex phase, and propose a THz LC element named forked polarization grating (FPG) [30,31]. The specifically designed LC directors with gradient rotation are implemented using photoalignment technology. The generated THz vortex beams are characterized with a THz imaging system. The resultant THz vortex beams with opposite circular polarization and *m* can be directly and simultaneously separated from undesirable beam components. Thus, a high mode purity can be obtained, and the polarization controllability feature can also be verified. This work provides a practical strategy for generating, separating and polarizing THz vortex beams, and promotes applications in numerous THz fields.

2. Principles and Experiments

2.1. Principles

Here, we introduce a blazed phase into common spiral phase, and the integrated phase profile obeys the following equation in the *x-y* plane:

$$\Phi(x,y) = m\phi(x,y) - 2\pi x/\Lambda \tag{1}$$

The first term on the right-hand side describes a spiral phase, where *m* denotes the topological charge and $\phi(x,y) = \arctan(y/x)$ exhibits the local azimuthal angle in the *x-y* plane. The second term describes the introduced blazed phase, where Λ is the pitch. The calculated phase distributions of a spiral phase, a blazed phase and their integration with *m* = 1 and $\Lambda \approx 1.2$ mm are shown in Figure 1a–c, respectively. It can be seen that the integrated phase is fork-like, with a space-variant change.
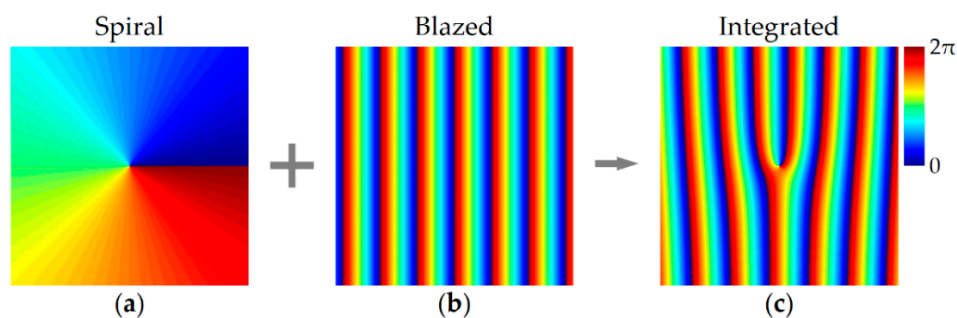

Figure 1. The calculated phase distribution of (**a**) a spiral phase; (**b**) a blazed phase; and (**c**) their integration with *m* = 1 and $\Lambda \approx 1.2$ mm.

Such forked phase profiles can be accomplished by PB phase, resulting from an LC wave plate with space-variant axis orientation (*α*) following:

$$\alpha(x,y) = \frac{\Phi(x,y)}{2} = \frac{1}{2}m\phi(x,y) - \pi x/\Lambda \tag{2}$$

The LC wave plates with such gradient-rotation directors is denoted LC FPG. The diffraction property can be theoretically analyzed through Jones matrix calculation [32]. The Jones matrix for such an FPG is given by:

$$
\begin{aligned}
\mathbf{J}(x,y) &= \mathbf{R}(-\alpha) \cdot \begin{bmatrix} \exp(-i\Gamma/2) & 0 \\ 0 & \exp(i\Gamma/2) \end{bmatrix} \cdot \mathbf{R}(\alpha) \\
&= \cos\zeta \mathbf{I} - i\sin\zeta \begin{bmatrix} \cos 2\alpha(x,y) & \sin 2\alpha(x,y) \\ \sin 2\alpha(x,y) & -\cos 2\alpha(x,y) \end{bmatrix}
\end{aligned}
\tag{3}
$$

where $\mathbf{I}$ is the identity matrix, $\zeta = \pi\Delta n d/\lambda$ is the normalized retardation (i.e., half of the phase retardation Γ), Δn is the LC birefringence, d is the cell gap and λ is the free-space wavelength. Consider a circularly polarized beam; it can be described as $\mathbf{E}_{\text{in}} = \chi^{(\pm)} = 1/\sqrt{2}\begin{pmatrix} 1 & \pm i \end{pmatrix}^{\text{T}}$, corresponding to left (+) and right (–) circular polarization states. After passing through such an LC FPG, the emerging wave can be expressed as:

$$
\begin{aligned}
\mathbf{D}(x,y) &= \mathbf{J}(x,y)\mathbf{E}_{\text{in}}(x,y) \\
&= \cos\zeta \cdot \chi^{(\pm)} - i\sin\zeta \cdot \exp\{\pm im \cdot \phi(x,y) \mp i2\pi x/\Lambda\} \cdot \chi^{(\mp)}
\end{aligned}
\tag{4}
$$

The far-field electric field of the *n*th diffraction order is:

$$
\begin{aligned}
\mathbf{D}_n &= \frac{1}{\Lambda}\int_0^{\Lambda} \mathbf{D}(x,y)e^{-i2\pi nx/\Lambda}\mathrm{d}x \\
&= \cos\zeta\delta_n\chi^{(\pm)} - i\sin\zeta\delta_{n\pm1}\exp\{\pm im \cdot \phi(x,y)\}\chi^{(\mp)}
\end{aligned}
\tag{5}
$$

Therefore, the diffraction efficiency $\eta_n = |\mathbf{D}_n|_2/|\mathbf{E}_{\text{in}}|^2$. We obtain

$$
\eta_0 = \cos^2\zeta \tag{6}
$$

$$
\eta_{\pm1} = \left|\left\langle \chi^{(\mp)} \middle| \Psi \right\rangle\right|^2 \sin^2\zeta \tag{7}
$$

$$
\eta_n = 0 (n \neq 0, \pm1) \tag{8}
$$

where $\left|\left\langle \chi^{(\mp)} \middle| \Psi \right\rangle\right|^2$ is the fraction of the input power in each $\chi^{(\mp)}$ spin eigenstate, and Ψ is the normalized input wave function. It can be seen that the FPG has only three diffraction orders: $\pm$1st orders are always circularly polarized and orthogonal to each other with OAM of opposite *m*; and 0th order is a Gaussian mode with the same polarization as the input beam. The intensity distribution among these three orders depends on the phase retardation and the incident polarization.

2.2. Experiments

A digital micro-mirror device-based dynamic micro-lithography setup is utilized to perform a multi-step partly-overlapping exposure (see details in Ref. [33]) in the LC cell placed at the image plane of the system. The quasi-continuous gradient-rotation director distribution corresponding to the designed LC FPG is transferred to the photoalignment layers. After the LC material NJU-LDn-4 (with a birefringence greater than 0.3 in the range of 0.5~2.5 THz [34]) is infiltrated, the LC FPG sample is obtained.

The stick in Figure 2a schematically shows the local director orientation of an LC FPG corresponding to Figure 1c. LC directors vary continuously and periodically, which can be further proved by the photo under crossed polarizers, as shown in Figure 2b. The dark domains indicate regions with LC directors approximately parallel to the polarizer or analyzer, while the bright domains correspond to regions with LC directors around 45° with respect to the polarizer/analyzer. The brightness changes continuously, consistent with the calculated director distribution.

To characterize the performance of the THz LC FPG, a THz digital holographic imaging system [35] is utilized, as schematically depicted in Figure 3. A linearly polarized THz beam with 3 mm diameter is excited and collimated to pass through a 1 THz quarter-wave plate (TQWP), which is used to control the incident polarization, and then illuminates on the center of the LC FPG sample. By employing a half-wave plate (HWP) and a polarizer (P) to adjust the probe polarization in the path of the probe beam, we can measure different polarization components of the emerging THz waves. The probe beam is reflected onto the ZnTe crystal (i.e., detecting crystal) by a 50/50 non-polarization beam splitter (BS). In the detection crystal, the probe polarization is modulated by the THz field to carry two-dimensional THz information, due to a linear electro-optic effect. The reflected probe beam is sent into the imaging module of the system, which consists of a QWP, a Wollaston prism (PBS), two lenses (L1 and L2), and a CCD camera with a 4 Hz frame rate for measuring the variation in the probe polarization, which is synchronous with the THz beam pumping. The imaging module can capture the image of the probe beam and extract the two-dimensional THz information by using dynamic subtraction and balanced electro-optic detection techniques [36,37]. A series of THz images in the time domain is acquired, and subsequently, the amplitude and phase information of each spectral component can be extracted by implementing Fast Fourier transformation.
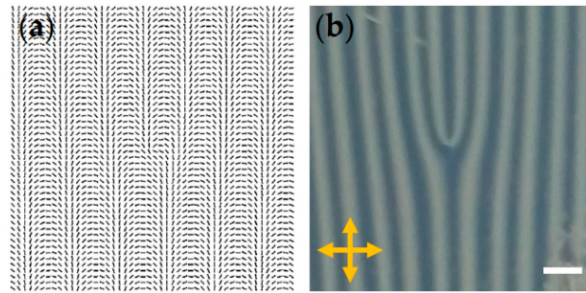

Figure 2. (**a**) The scheme of the director distribution of an LC FPG with $m = 1$ and $\Lambda \approx 1.2$ mm; (**b**) corresponding photo under crossed polarizers; the scale bar is 1 mm.
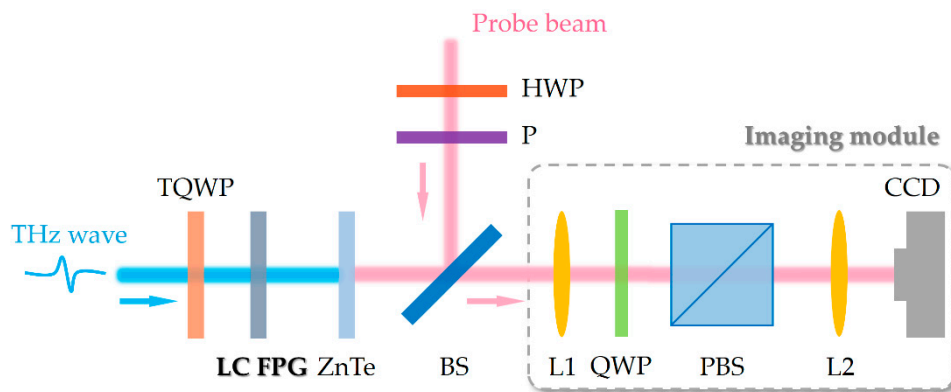

Figure 3. The scheme of the THz digital holographic imaging system.

3. Results and Discussion

By adjusting the polarization of the probe beam, we can detect two orthogonal linearly polarized components of the output THz beam. When the incident polarization is horizontal, the incident beam diffracts into three orders. According to the analysis above, the ±1st orders are left/right circularly polarized (LCP/RCP) vortex beams with $m = \mp 1$, and the 0th order is a Gaussian beam. The intensity pattern of the detected vertically polarized components of the diffracted beams at 1 THz is shown in Figure 4a. The two donut-like profiles correspond to the ±1st orders. The absence of the 0th order verifies that it has the same polarization as the input beam (i.e., horizontal polarization).

The ±1st orders are vortex beams with opposite twist directions of helical phase, and are diffracted in two symmetric directions. Therefore, the detected phase distributions for these two orders are opposite spiral phases integrated with opposite tilt phases, forming two mirror-inverted fork-like patterns, as shown in Figure 4b. When we adjust the TQWP to make the incident THz wave LCP, only RCP −1st order with $m = +1$ and the 0th order exist. The measured intensity pattern for vertical component at 1 THz is shown in Figure 4c. On the other hand, for RCP THz beam, only LCP +1st order with $m = −1$ and the 0th order are revealed in Figure 4d.
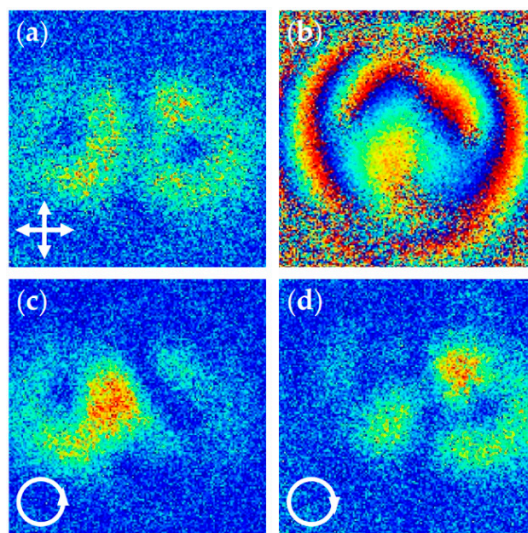

Figure 4. (**a**) Intensity and (**b**) phase distribution of the detected vertically polarized components of the diffracted beams at 1 THz for horizontally polarized incident; the measured intensity pattern for vertical polarization component for (**c**) LCP and (**d**) RCP incident THz beam.

The THz LC FPG can generate THz vortex beams with opposite circular polarization and topological charges, which are directly separated from the undesirable 0th order. Due to the inherent diffraction property of the fork grating, the generated THz vortex beams are pure. Via tuning the incident polarization, a switch between ±1st orders can be realized. In addition, the absorption coefficients κ_o and κ_e of the LC NJU-LDn-4 are 0.05 and 0.03, respectively, in the range of 0.5~2.5 THz [34]. We take the average value of absorption coefficient as 0.04 for such a continuously space-variant director distribution, and the calculated absorption loss at 1 THz is approximately 34% of the total input. The phase retardation of the LC layer is about 0.5π for 1 THz, which limits the diffraction efficiency (~40% of the total output). This can be improved by increasing the thickness of the LC layer and optimizing the birefringence of the LC material for a larger phase retardation. Compared to other THz devices such as those based on low-loss THz polymers, the tunability of LC makes it possible to realize electro-optical switching and achieve maximum efficiency at different frequencies. Few-layer porous graphene films can be used as high-transparent electrodes [27,29] to drive such LC devices.

4. Materials and Methods

Photoalignment is suitable for the high-resolution multi-domain LC alignment [38]. Here, a polarization-sensitive medium sulfonic azo dye SD1 (Dai-Nippon Ink and Chemicals, Tokyo, Japan) is used as the photoalignment agent. SD1 molecules tend to reorient their absorption oscillators perpendicular to the polarization direction when illuminated by a linearly polarized UV and then consequently guide the LC orientations [39].

Fused silica glass substrates (1.5 × 2 cm^2, 0.8 mm thickness) are oxygen-plasma cleaned and then spin-coated with a 0.3% solution of SD1 in dimethylformamide. Two SD1-coated substrates are

assembled together and sealed with epoxy glue to form an empty cell. The cell gap is controlled by 250 μm-thick Mylar films.

5. Conclusions

We fabricate a THz LC FPG by photopatterning a large birefringent LC into specific gradient-rotation directors, and further characterize it with a THz imaging system. The FPG can simultaneously generate and separate pure THz vortices with opposite circular polarization and opposite *m*. The polarization controllability of the THz vortex beam is also demonstrated. This work supplies a compact and practical method for THz vortex beam generation, and may facilitate various THz applications including THz imaging, sensing and communication.

Author Contributions: W.H. and Y.-Q.L. conceived the original idea; S.-J.G., Z.-X.S., and P.C. fabricated the sample, analyzed the data and wrote the manuscript; X.-K.W. and Y.Z. performed the THz analysis; X.L. made a constructive analyzing of the LC material; X.L. and W.H. co-supervised and directed the research.

Conflicts of Interest: The authors declare no conflict of interest.

References

1. Torres, J.P.; Torner, L. *Twisted Photons: Applications of Light with Orbital Angular Momentum*; John Wiley & Sons: Weinheim, Germany, 2011.
2. Yao, A.M.; Padgett, M.J. Orbital angular momentum: Origins, behavior and applications. *Adv. Opt. Photonics* **2011**, *3*, 161–204. [CrossRef]
3. Allen, L.; Beijersbergen, M.W.; Spreeuw, R.; Woerdman, J. Orbital angular momentum of light and the transformation of Laguerre-Gaussian laser modes. *Phys. Rev. A* **1992**, *45*, 8185. [CrossRef] [PubMed]
4. Padgett, M.; Bowman, R. Tweezers with a twist. *Nat. Photonics* **2011**, *5*, 343–348. [CrossRef]
5. Wang, J.; Yang, J.Y.; Fazal, I.M.; Ahmed, N.; Yan, Y.; Huang, H.; Ren, Y.; Yue, Y.; Dolinar, S.; Tur, M.; et al. Terabit free-space data transmission employing orbital angular momentum multiplexing. *Nat. Photonics* **2012**, *6*, 488–496. [CrossRef]
6. Lei, T.; Zhang, M.; Li, Y.R.; Jia, P.; Liu, G.N.; Xu, X.G.; Li, Z.H.; Min, C.J.; Lin, J.; Yu, C.Y.; et al. Massive individual orbital angular momentum channels for multiplexing enabled by dammann gratings. *Light Sci. Appl.* **2015**, *4*, e257. [CrossRef]
7. Zhou, Z.Y.; Liu, S.L.; Li, Y.; Ding, D.S.; Zhang, W.; Shi, S.; Dong, M.X.; Shi, B.S.; Guo, G.C. Orbital angular momentum-entanglement frequency transducer. *Phys. Rev. Lett.* **2016**, *117*, 103601. [CrossRef] [PubMed]
8. D'Ambrosio, V.; Nagali, E.; Walborn, S.P.; Aolita, L.; Slussarenko, S.; Marrucci, L.; Sciarrino, F. Complete experimental toolbox for alignment-free quantum communication. *Nat. Commun.* **2012**, *3*, 961. [CrossRef] [PubMed]
9. Wang, X.L.; Cai, X.D.; Su, Z.E.; Chen, M.C.; Wu, D.; Li, L.; Liu, N.L.; Lu, C.Y.; Pan, J.W. Quantum teleportation of multiple degrees of freedom of a single photon. *Nature* **2015**, *518*, 516–519. [CrossRef] [PubMed]
10. Ferguson, B.; Zhang, X.C. Materials for terahertz science and technology. *Nat. Mater.* **2002**, *1*, 26–33. [CrossRef] [PubMed]
11. Zhang, X.C.; Xu, J. *Introduction to THz Wave Photonics*; Springer: Boston, MA, USA, 2010.
12. Sanvitto, D.; Marchetti, F.; Szymańska, M.; Tosi, G.; Baudisch, M.; Laussy, F.; Krizhanovskii, D.; Skolnick, M.; Marrucci, L.; Lemaitre, A. Persistent currents and quantized vortices in a polariton superfluid. *Nat. Phys.* **2010**, *6*, 527–533. [CrossRef]
13. Koenig, S.; Lopez-Diaz, D.; Antes, J.; Boes, F.; Henneberger, R.; Leuther, A.; Tessmann, A.; Schmogrow, R.; Hillerkuss, D.; Palmer, R.; et al. Wireless sub-THz communication system with high data rate. *Nat. Photonics* **2013**, *7*, 977–981. [CrossRef]
14. Miyamoto, K.; Suizu, K.; Akiba, T.; Omatsu, T. Direct observation of the topological charge of a terahertz vortex beam generated by a Tsurupica spiral phase plate. *Appl. Phys. Lett.* **2014**, *104*, 261104. [CrossRef]

15. Wang, X.; Shi, J.; Sun, W.; Feng, S.; Han, P.; Ye, J.; Zhang, Y. Longitudinal field characterization of converging terahertz vortices with linear and circular polarizations. *Opt. Express* **2016**, *24*, 7178–7190. [CrossRef] [PubMed]

16. Xie, Z.; Wang, X.; Ye, J.; Feng, S.; Sun, W.; Akalin, T.; Zhang, Y. Spatial terahertz modulator. *Sci. Rep.* **2013**, *3*, 3347. [CrossRef]

17. Knyazev, B.; Choporova, Y.Y.; Mitkov, M.; Pavelyev, V.; Volodkin, B. Generation of terahertz surface plasmon polaritons using nondiffractive Bessel beams with orbital angular momentum. *Phys. Rev. Lett.* **2015**, *115*, 163901. [CrossRef] [PubMed]

18. He, J.; Wang, X.; Hu, D.; Ye, J.; Feng, S.; Kan, Q.; Zhang, Y. Generation and evolution of the terahertz vortex beam. *Opt. Express* **2013**, *21*, 20230–20239. [CrossRef] [PubMed]

19. Imai, R.; Kanda, N.; Higuchi, T.; Konishi, K.; Kuwata-Gonokami, M. Generation of broadband terahertz vortex beams. *Opt. Lett.* **2014**, *39*, 3714–3717. [CrossRef] [PubMed]

20. Minasyan, A.; Trovato, C.; Degert, J.; Freysz, E.; Brasselet, E.; Abraham, E. Geometric phase shaping of terahertz vortex beams. *Opt. Lett.* **2017**, *42*, 41–44. [CrossRef] [PubMed]

21. Chen, C.Y.; Pan, C.L.; Hsieh, C.F.; Lin, Y.F.; Pan, R.P. Liquid-crystal-based terahertz tunable Lyot filter. *Appl. Phys. Lett.* **2006**, *88*, 101107. [CrossRef]

22. Ho, I.C.; Pan, C.L.; Hsieh, C.F.; Pan, R.P. Liquid-crystal-based terahertz tunable Solc filter. *Opt. Lett.* **2008**, *33*, 1401–1403. [CrossRef] [PubMed]

23. Wilk, R.; Vieweg, N.; Kopschinski, O.; Koch, M. Liquid crystal based electrically switchable Bragg structure for THz waves. *Opt. Express* **2009**, *17*, 7377–7382. [CrossRef] [PubMed]

24. Lin, X.W.; Wu, J.B.; Hu, W.; Zheng, Z.G.; Wu, Z.J.; Zhu, G.; Xu, F.; Jin, B.B.; Lu, Y.Q. Self-polarizing terahertz liquid crystal phase shifter. *AIP Adv.* **2011**, *1*, 032133. [CrossRef]

25. Shrekenhamer, D.; Chen, W.C.; Padilla, W.J. Liquid crystal tunable metamaterial absorber. *Phys. Rev. Lett.* **2013**, *110*, 177403. [CrossRef] [PubMed]

26. Ge, S.; Liu, J.; Chen, P.; Hu, W.; Lu, Y. Tunable terahertz filter based on alternative liquid crystal layers and metallic slats. *Chin. Opt. Lett.* **2015**, *13*, 120401. [CrossRef]

27. Wang, L.; Lin, X.W.; Hu, W.; Shao, G.H.; Chen, P.; Liang, L.J.; Jin, B.B.; Wu, P.H.; Qian, H.; Lu, Y.N.; et al. Broadband tunable liquid crystal terahertz waveplates driven with porous graphene electrodes. *Light Sci. Appl.* **2015**, *4*, e253. [CrossRef]

28. Isic, G.; Vasic, B.; Zografopoulos, D.C.; Beccherelli, R.; Gajic, R. Electrically tunable critically coupled terahertz metamaterial absorber based on nematic liquid crystals. *Phys. Rev. Appl.* **2015**, *3*, 064007. [CrossRef]

29. Ge, S.; Chen, P.; Shen, Z.; Sun, W.; Wang, X.; Hu, W.; Zhang, Y.; Lu, Y. Terahertz vortex beam generator based on a photopatterned large birefringence liquid crystal. *Opt. Express* **2017**, *25*, 12349–12356. [CrossRef] [PubMed]

30. Chen, P.; Wei, B.-Y.; Ji, W.; Ge, S.-J.; Hu, W.; Xu, F.; Chigrinov, V.; Lu, Y.-Q. Arbitrary and reconfigurable optical vortex generation: A high-efficiency technique using director-varying liquid crystal fork gratings. *Photonics Res.* **2015**, *3*, 133–139. [CrossRef]

31. Zhang, X.D.; Su, Y.H.; Ni, J.C.; Wang, Z.Y.; Wang, Y.L.; Wang, C.W.; Ren, F.F.; Zhang, Z.; Fan, H.; Zhang, W.J.; et al. Optical superimposed vortex beams generated by integrated holographic plates with blazed grating. *Appl. Phys. Lett.* **2017**, *111*, 061901. [CrossRef]

32. Li, Y.; Kim, J.; Escuti, M.J. Orbital angular momentum generation and mode transformation with high efficiency using forked polarization gratings. *Appl. Opt.* **2012**, *51*, 8236–8245. [CrossRef] [PubMed]

33. Ji, W.; Lee, C.H.; Chen, P.; Hu, W.; Ming, Y.; Zhang, L.; Lin, T.H.; Chigrinov, V.; Lu, Y.Q. Meta-q-plate for complex beam shaping. *Sci. Rep.* **2016**, *6*, 25528. [CrossRef] [PubMed]

34. Wang, L.; Lin, X.W.; Liang, X.; Wu, J.B.; Hu, W.; Zheng, Z.G.; Jin, B.B.; Qin, Y.Q.; Lu, Y.Q. Large birefringence liquid crystal material in terahertz range. *Opt. Mater. Express* **2012**, *2*, 1314–1319. [CrossRef]

35. Wang, B.; Quan, B.; He, J.; Xie, Z.; Wang, X.; Li, J.; Kan, Q.; Zhang, Y. Wavelength de-multiplexing metasurface hologram. *Sci. Rep.* **2016**, *6*, 35657. [CrossRef] [PubMed]

36. Jiang, Z.; Xu, X.; Zhang, X.C. Improvement of terahertz imaging with a dynamic subtraction technique. *Appl. Opt.* **2000**, *39*, 2982–2987. [CrossRef] [PubMed]

37. Wang, X.; Cui, Y.; Sun, W.; Ye, J.; Zhang, Y. Terahertz polarization real-time imaging based on balanced electro-optic detection. *J. Opt. Soc. Am. A* **2010**, *27*, 2387–2393. [CrossRef] [PubMed]

38. Wu, H.; Hu, W.; Hu, H.C.; Lin, X.W.; Zhu, G.; Choi, J.W.; Chigrinov, V.; Lu, Y.Q. Arbitrary photo-patterning in liquid crystal alignments using DMD based lithography system. *Opt. Express* **2012**, *20*, 16684–16689. [CrossRef]

39. Chigrinov, V.; Pikin, S.; Verevochnikov, A.; Kozenkov, V.; Khazimullin, M.; Ho, J.; Huang, D.D.; Kwok, H.S. Diffusion model of photoaligning in azo-dye layers. *Phys. Rev. E* **2004**, *69*, 061713. [CrossRef] [PubMed]